



HAL
open science

Combining experimental and theoretical tools to probe radio-oxidation products in polyethylene

Muriel Ferry, Yunho Ahn, Florian Le Dantec, Yvette Ngonon-Ravache, Guido Roma

► **To cite this version:**

Muriel Ferry, Yunho Ahn, Florian Le Dantec, Yvette Ngonon-Ravache, Guido Roma. Combining experimental and theoretical tools to probe radio-oxidation products in polyethylene. *Polymers*, 2023, 15, pp.1537. 10.3390/polym15061537 . cea-04598123

HAL Id: cea-04598123

<https://cea.hal.science/cea-04598123>

Submitted on 3 Jun 2024

HAL is a multi-disciplinary open access archive for the deposit and dissemination of scientific research documents, whether they are published or not. The documents may come from teaching and research institutions in France or abroad, or from public or private research centers.

L'archive ouverte pluridisciplinaire **HAL**, est destinée au dépôt et à la diffusion de documents scientifiques de niveau recherche, publiés ou non, émanant des établissements d'enseignement et de recherche français ou étrangers, des laboratoires publics ou privés.



Distributed under a Creative Commons Attribution 4.0 International License

Combining experimental and theoretical tools to probe radio-oxidation products in polyethylene

Muriel Ferry¹, Yunho Ahn², Florian Le Dantec¹, Yvette Ngono³ and Guido Roma^{2,*}

¹ Université Paris-Saclay, CEA, Service de Physico-Chimie (SPC), 91191 Gif sur Yvette, France; muriel.ferry@cea.fr (M.F.); ledantec.florian@gmail.com (F.L.D.)

² Université Paris-Saclay, CEA, Service de Recherches en Corrosion et Comportement des Matériaux, SRMP, 91191 Gif sur Yvette, France; yunho.ahn@cea.fr (Y.A.); guido.roma@cea.fr (G.R.)

³ Normandie Univ, ENSICAEN, UNICAEN, CEA, CNRS, CIMAP, UMR 6252, BP 5133 Caen Cedex 05 F-14070 France; yvette.ngono-ravache@cea.fr (Y.N.)

* Correspondence: guido.roma@cea.fr (G.R.)

Abstract: Polyethylene is one of the most used polymers in a variety of sectors. A typical technique used to assess ageing is infrared spectroscopy. Under oxidation, the region of the spectrum which is mostly studied is the one containing the carbonyl signature. However, various carbonyl groups contribute to the carbonyl peak: ketones, aldehydes, esters, lactones, carboxylic acids, and more. A usual procedure to quantify each of them is the deconvolution of experimental peaks based on experimental assignments of infrared bands. In this paper we complement such procedure, applied on two polyethylene types, with extended density functional theory (DFT) calculations of infrared spectra, using a polyethylene model mimicking the main features of a semicrystalline polymer. We compare theoretical frequencies and infrared intensities with parameters extracted from the literature and used to, eventually, estimate concentrations. We provide an alternative estimation entirely based on theoretical data, showing that DFT can be a valuable tool to analyse, or at least complement, experimental data to assess polymer ageing. The comparison of different deconvolution procedures raises the question of the contribution of conjugated ketones in the global carbonyl buildup, as well as that of ketones/alcohols pairs, or the relative concentration of esters and aldehydes.

Keywords: polyethylene; radio-oxidation; infrared spectroscopy ; carbonyl ; density functional theory ; ab initio

Citation: Combining experimental and theoretical tools to probe radio-oxidation products in polyethylene. *Polymers* **2021**, *1*, 0. <https://doi.org/>

Received:
Accepted:
Published:

Publisher's Note: MDPI stays neutral with regard to jurisdictional claims in published maps and institutional affiliations.

Copyright: © 2023 by the authors. Submitted to *Polymers* for possible open access publication under the terms and conditions of the Creative Commons Attribution (CC BY) license (<https://creativecommons.org/licenses/by/4.0/>).

1. Introduction

One of the most produced polymers is polyethylene, in its various forms (HDPE, LDPE, LLDPE) constituting roughly one fourth of total annual plastics world production [1]. The domains of applications span from everyday life food packaging, to electric cable insulation, to more niche, though important, sectors like the medical one (e.g., hips prothesis). Polyethylene is vulnerable to oxidation, whose concern depends on the application, its expected lifetime and the environmental conditions in which it is used. For example, the oxidation of PE in contact with biological tissues is a concern for medical applications [2]. Harsh environments (temperature, irradiation) constitute a threat for the lifetime of electric cables used in, e.g., nuclear power plants [3] (NPP).

We focus here on model materials similar to those used for the insulation of electric cables in NPP, in order to investigate the accumulation of oxidation defects under γ -irradiation, at doses typical of NPP ageing. Even model materials, in general, also contain additives like phenolic antioxidants, whose role is to delay the oxidation of the material. Understanding the role of the pristine microstructure on the ageing mechanism is important. For this reason we choose to compare LLDPE (linear low density polyethylene) with a crosslinked polyethylene (XLPE). The investigation conditions are,

35 for relatively high doses, representative of the environment of NPP [3,4] and, for dose
36 rates, corresponding to accelerated ageing experiments currently available [5–8].

37 Several experimental techniques have been used in order to characterise the accu-
38 mulation of oxidation species, in particular carbonyl species, in oxidized polyethylene.
39 Electronic paramagnetic resonance (EPR), for example, has been used since the early
40 days of irradiation studies of hydrocarbons to detect transient radical species [9], and has
41 been a very useful tool to characterise some radicals [10–13]. It is however a technique
42 insensitive to most stable final products, which do not carry an unpaired spin. Other op-
43 tical techniques can be used to probe carbonyl species, for example photoluminescence
44 (PL) [14,15] or Raman spectroscopy, but they are hardly able to distinguish, from each
45 other, the various carbonyl species that might be present in oxidized polyethylene.

46 Other techniques have been used, like NMR [16,17], however their sensitivity is
47 much lower than what can be considered the technique of choice for a fine characterisa-
48 tion of carbonyl species: Fourier transform infrared spectroscopy (FTIR) [18–23]. This
49 technique allows the detection of newly formed species in particular in the regions
50 of 3000–3600 cm^{-1} (hydroxyl, hydroperoxides), 1600–1800 cm^{-1} (carbonyl and insatu-
51 rations, C=O/C=C bonds). In spite of a lot of remarkable works, the deconvolution
52 of all contributions to, e.g., the experimental signature of carbonyls is far from being
53 straightforward.

54 Even this powerful tool suffers from limitations related, on the one hand, to the
55 choice of the carbonyl species to be inserted in the deconvolution procedures and,
56 on the other hand, to reliable assignment of characteristic frequencies and absorption
57 coefficients of each of the included chemical groups [23]. One of the difficulties is to
58 obtain reference data which are representative of the local atomic environment; the latter
59 is not even clearly defined, given the fact that samples of polymers to analyze contain
60 amorphous and crystalline phases. Moreover, even excluding the possibility of finding
61 carbonyl species in the crystalline regions —on the basis of the usual assumption that
62 oxygen cannot diffuse through the crystal— frequency and absorptivity can change
63 according to their localisation in the amorphous and/or at the interface between the
64 crystalline and the amorphous regions.

65 Our goal, in this work, is to complement experimental characterization by FTIR
66 with theoretical calculations of infrared spectra based on Density Functional Theory
67 (DFT). Calculation of harmonic vibrational frequencies in solids and molecules is based
68 on the calculation of the second derivative of the total energy *versus* displacements either
69 by finite differences or by linear response approaches [24]. For molecules, extensive tests
70 with various levels of theory suggest scaling factors to correct errors on the frequencies
71 which, nevertheless, only rarely exceed a few percent [25]. Calculations on phonon
72 frequencies of inorganic solids are in general within the same error range with respect to
73 experiments.

74 Intensities associated with a given eigenmode depend on the derivative of the
75 dipole moment with respect to the normal mode coordinate [26]. They can be calcu-
76 lated using DFT both for molecules and solids, through Born effective charges and the
77 phonons eigenvectors. Benchmarks on a set of small molecules show that DFT gives
78 results comparable to higher level quantum chemistry approaches at a much lower
79 cost [27]. While, as far as we know, no attempt was made to use IR frequencies and
80 intensities calculated with DFT in order to unravel experimental spectra of carbonyl
81 species in aliphatic polymers, such an approach has been applied to uracil, with a dy-
82 namic approach [28], and to hydroxyl containing minerals in order to rationalize their
83 behavior under pressure [29].

84 In this paper we combine DFT calculations of frequencies and IR intensities of
85 various carbonyl species in a model mimicking the interface between crystalline and
86 amorphous phases in PE, with experimental characterisation of γ -irradiated PE (LLDPE
87 and XLPE) using FTIR. In the following section (2) we give experimental (2.1, 2.1.1,
88 2.1.2) and theoretical (2.2) details of our approach. Then, we present the results in

89 section 3 where, after giving the main direct outcome of the experiments (3.1) and of
90 the calculations (3.2), we compare and combine them to obtain the evolution of the
91 concentration of various carbonyl species in the two sets of materials (section 3.3). In the
92 discussion accompanying the presentation of the results, we highlight the advantage of
93 combining theory and experiment in this kind of characterisation and underline some
94 open questions that arise from our comparison.

95 2. Materials and Methods

96 2.1. Experimental setup

97 2.1.1. Sample preparation

98 Linear Low Density Polyethylene LLDPE (with a density $\rho=0.918 \text{ g}\cdot\text{cm}^{-3}$) was
99 either only shaped as films or it was crosslinked using 1 phr of Dicumyl Peroxide (DCP).
100 The first step consists in producing a homogeneous mixture of the polymer and of the
101 crosslinking agent. Mixtures are made in a Haake thermoScientific twin-screw extruder,
102 the cells having a total volume of 69 cm^3 . They are prepared under air by heating the
103 cells up to 110°C and using a 50 rpm blade rotation speed, filling the Haake with LLDPE.
104 After LLDPE melting, the crosslinking agent is introduced and the mixture is left 5
105 minutes before removal of the twin-screw extruder. Crosslinking and shaping as films
106 are performed in one single stage in a hydraulic press Polystat 200 T heater from Servitec.
107 The following protocol is applied, for pure LLDPE as for LLDPE + DCP: the material is
108 heated up to 170°C then introduced in a $250 \mu\text{m}$ spacer, which is itself introduced in the
109 hydraulic press until temperature homogenization is achieved. A pressure of 50 bar is
110 applied for 30 seconds, then it is increased up to 200 bars by 50 bars steps. After keeping
111 the polymer for 15 minutes at 200 bars, the film is finally removed from the hydraulic
112 press and let to cool down before collecting the sample. Hereafter, pure polymer is
113 referred to as LLDPE whereas LLDPE + DCP is referred to as XLPE. Characterization of
114 both materials was carried out and the outcomes are described in the Supplementary
115 Information. The following sum up can be given: LLDPE base material contains a small
116 proportion of Irganox 1076 and its gel fraction is null even after shaping. XLPE contains
117 the same primary antioxidant but also DCP decomposition products; its gel fraction is
118 equal to $67 \pm 1 \%$ before irradiation.

119 2.1.2. Irradiation

To perform irradiations in controlled atmospheric conditions, each sample was introduced in a glass container of known volume. Ampoules were evacuated using a vacuum line and then filled with reconstituted air (20.0% O_2 , 77.99% N_2 , 2.01% Kr), krypton being used as a tracer to determine the final pressure. Pictures of similar samples in their glass containers can be found in a previous paper [30]. Sample masses were estimated to obtain, at the end of the irradiation, a final H_2 content of about 1 vol%. This protocol is performed to allow the quantification of the radiolysis gases: the results, out of the scope of this article, will be presented elsewhere. γ -irradiations were performed using ^{60}Co sources at the Poseidon facility of LABRA (Saclay, France). Dosimetry was performed using a UNIDOS PTW dosimeter equipped with a calibration chamber adjusted every two years by the CEA's LNHB laboratory. No electronic correction was made to take into account the electronic density difference between water and the polymers. Uncertainties on given doses are less than 6%. Dose rates and doses at which FTIR spectra were collected, are gathered in Table 1. As irradiations have been performed under oxidative atmosphere, the critical thickness not to be exceeded to ensure homogeneous oxidation conditions through the polymer thickness, e_c has to be estimated. We used the Gillen & Clough [31] relation, given by

$$e_c = \sqrt{\frac{8 \cdot p \cdot P(\text{O}_2)}{G(-\text{O}_2) \cdot I}}, \quad (1)$$

Table 1: Irradiation conditions.

Nominal dose (kGy)	Dose rate (Gy/h)	Real dose (kGy)
12	1.07	11.96 ± 0.72
24	1.07	24.02 ± 1.44
50	1.06	49.98 ± 3.00
100	1.06	99.98 ± 6.00

Table 2: FTIR band assignments in the carbonyl area. We note by ν_{exp}^* the assigned experimental wavenumber (from the reference in the last column) and with ν^{min} and ν^{max} the minimum and maximum values allowed in the deconvolution procedure.

FTIR band assignment	ν_{exp}^* [cm ⁻¹]	Degree of freedom		Reference
		ν^{min} [cm ⁻¹]	ν^{max} [cm ⁻¹]	
Lactone	1785	1783	1787	Ref. [33]
Ketone+alcohol	1706	1704	1708	Theory, this work
Free carboxylic acid or Peracid Ester	1756	1754	1758	Refs. [33],[34]
Aldehyde	1740	1738	1742	Ref. [35]
Ketone	1730	1728	1732	Ref. [35]
H-bonded carboxylic acid	1718	1716	1720	Ref. [35]
Conjugated ketone	1710	1708	1712	Ref. [36]
	1685	1683	1687	Ref. [32]

120 where $P(O_2)$ is the oxygen pressure (in atm) in the irradiation cell, p is the oxygen
 121 permeation in the polymer (in mol·cm²·kg⁻¹·atm⁻¹·s⁻¹), I is the dose rate (in Gy·s⁻¹),
 122 and $G(-O_2)$ is the oxygen consumption radiation chemical yield (in mol·J⁻¹). e_c was
 123 estimated to be about 150 μm. Nominal film thicknesses being about 250 μm, it has
 124 thus to be supposed that irradiations are not performed homogeneously as far as the
 125 oxidation is concerned.

126 2.1.3. Fourier Transform Infrared Spectroscopy

127 Fourier Transform Infrared (FTIR) spectra of the polymers were acquired using a
 128 Bruker Tensor 27 spectrometer equipped with a Bruker Platinum single reflection dia-
 129 mond attenuated total reflectance (ATR) accessory and a DTGS (Deuterated TriGlycine
 130 Sulfate) detector. Spectra were recorded between 4000 and 600 cm⁻¹ at a resolution of
 131 2 cm⁻¹ with 64 accumulated scans.

132 Deconvolution is one of the two techniques usually employed to discriminate the
 133 absorption bands, linked to different functional groups, forming a single broad infrared
 134 peak [32]. In this study, the fitting is performed on the carbonyl broad peak which
 135 grows in PE during radio-oxidation. The fitting was performed assuming the FTIR band
 136 assignments given in Table 2, allowing a certain degree of freedom on the positions of
 137 the peak maxima and widths.

138 Deconvolutions were carried out for both materials but only at the two higher
 139 doses listed in Table 1, as the carbonyl signal at 12 and 24 kGy was too weak to obtain
 140 reliable results. The baseline to be removed was determined in the area 1650-1800 cm⁻¹.
 141 The fitting function used is a combination of Gaussian functions, which corresponds to

142 the assumption that linewidths stem essentially from disorder, i.e., that new bonds are
143 formed mainly in the amorphous phase.

144 For each set of data we carried out four alternative deconvolutions, with different
145 constraints on the FWHM of the gaussian components. The reason for that is, first, to
146 check how the quality of the fit depends on this parameter and, second, to relate this
147 parameter to the spread of the frequencies obtained theoretically while varying the local
148 environment of each of the considered chemical species. The constraints on the FWHM,
149 assumed to be the same for all chemical groups, were: 5-18 cm^{-1} , 10-20 cm^{-1} , 15-25
150 cm^{-1} and 20-30 cm^{-1} . Experimental analysis generally assumes infrared band widths
151 do not exceed 15 cm^{-1} . However, our theoretical results suggest that bands can be larger.
152 Further details are provided in the Supplementary Information.

153 In addition to the deconvolutions carried out with experimental reference frequen-
154 cies, a deconvolution of the experimental results was performed with the frequencies
155 obtained by DFT calculations discussed later. In this case the peaks central position were
156 given the same degree of freedom as for experimental reference frequencies, while the
157 widths of the gaussians were allowed to span the range 10 to 20 cm^{-1} .

158 In the following we will show only the result of one deconvolution (the one with
159 constrained FWHM between 10 and 20 cm^{-1}), but further details are given in the
160 Supplementary Information.

161 2.2. Theoretical approach

162 Our theoretical approach of the infrared spectrum of polyethylene containing
163 carbonyl defects is based on density functional theory (DFT). Before describing the
164 technical details of the theoretical framework we discuss the model used for polyethylene,
165 in order to represent both the crystalline and the amorphous regions, and their interface.
166 We relied on a slab supercell including a thin crystalline lamella separated by its periodic
167 images, in the direction perpendicular to the lamella surface, by a region which is
168 empty space except for a single chain connecting the two lamella surfaces. This model,
169 containing 150 atoms, is a variant of the model described in detail in [37]; the modification
170 consists in the connecting chain, which was branched on each surface by removing a
171 hydrogen atom. A view of this model can be seen in figure 1. The model was fully
172 relaxed by keeping fixed the in-plane lattice parameter of the orthorhombic crystal and,
173 for the out-of-plane lattice parameter, we kept the value used in [37]. We note that this
174 gives an overall density (0.88 g/cm^{-3}) which is close to typical experimental values for
175 LLDPE.

176 Total energy calculations were performed with norm conserving pseudopotentials
177 and a plane wave basis set with a kinetic-energy cutoff of 80 Rydberg. A Γ -centered
178 $2 \times 3 \times 2$ Monkhorst-Pack \mathbf{k} -grid was used for representing screening. The atomic struc-
179 tures were relaxed down to a force threshold of 10^{-4} Rydberg/Bohr. The chosen ex-
180 change correlation (xc) functional is the optB86b van der Waals functional [38] providing
181 a satisfactory description of dispersion forces in polyethylene [39].

The model's eigenfrequencies and infrared activities were calculated in the frame-
work of density functional perturbation theory (DFPT) [24] using the `ph.x` module of
the QUANTUM-ESPRESSO software package [40]. The infrared activity for mode ν , I_ν , is
obtained from the DFPT Born effective charges $Z_{\alpha,\beta}^i$ and phonon displacements $u_{\nu,\beta}^i$ as

$$I_\nu = \sum_{\alpha} \left| \sum_{i,\beta} Z_{\alpha,\beta}^i u_{\nu,\beta}^i \right|^2 \quad (2)$$

182 where α and β are cartesian directions and i is the label of the atom in the cell. We note
183 that this quantity, proportional to the contribution of a single mode to the IR absorption
184 cross sections ($\sigma_{IR}(\nu)$), is closely related to the molar extinction coefficient, indicated
185 by $\epsilon_{IR}(\nu)$, through $\sigma_{IR}(\nu) = \log(10) \times 10^3 / N_A \times \epsilon_{IR}(\nu)$, where N_A is the Avogadro
186 number.

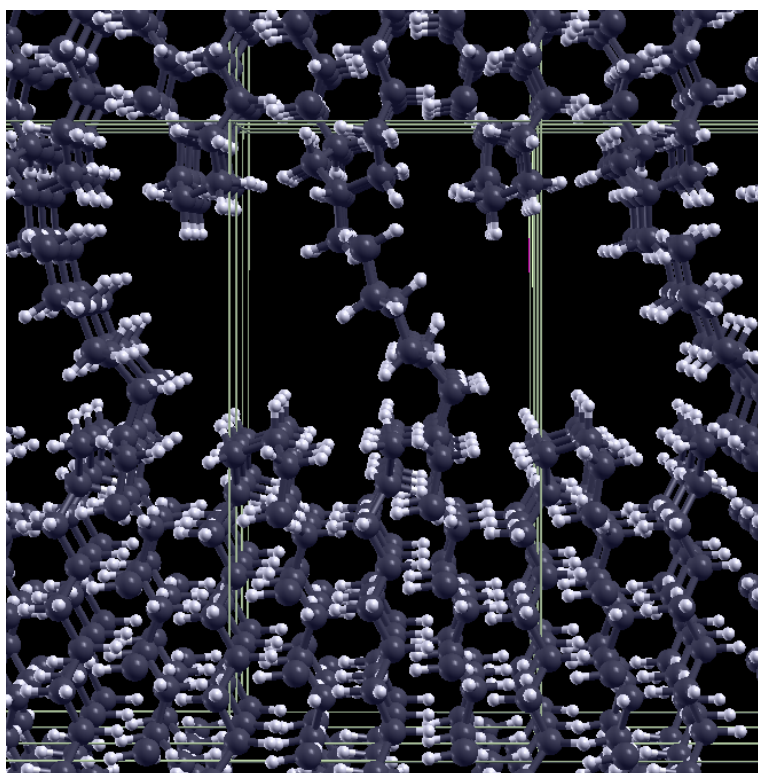


Figure 1. The PE model used for DFT calculations; the periodically repeated unit cell, including a thin crystalline lamella with two surfaces connected by an alky chain, is shown. The parameters of the orthorhombic cell, containing 151 atoms, are 9.72, 6.96 and 19.96 Å.

187 Carbonyl defects of various types were introduced in the lamellar model just
188 described at various possible positions (one at a time); for example, for carboxylic acids
189 the insertion procedure (somewhat more complex than for other groups) consisted
190 in taking three consecutive carbons, saturating the first with an additional hydrogen,
191 removing the second with the two attached hydrogens, and, for the third, substituting
192 the two attached hydrogens with an oxygen atom and an OH group. After the insertion
193 of the carbonyl group the structure was then fully relaxed before performing phonon
194 calculations. In order to classify the different insertion sites, the crystal bulk, the surface,
195 and the amorphous region separating the two surfaces, were determined on the basis of
196 the in-plane averaged atomic density, as shown in figure 2.

197 2.3. Calculation of carbonyl concentrations

198 The concentration c of the various carbonyl species in the four PE samples have
199 been extracted from the gaussian height, outcome of the deconvolution, through the
200 Beer-Lambert law ($A = \epsilon lc$), where ϵ is the molar extinction coefficient at the relevant
201 frequency, assuming that the heights are proportional to the absorbance A . The path
202 length l corresponds to the effective penetration depth.

203 FTIR-ATR spectra were recorded in Attenuated Total Reflectance. Using this kind
204 of module, the depth of penetration d_p and the effective penetration d_e can be calculated
205 according to the equations in Ref. [23], using the refractive index of the ATR crystal
206 (diamond, $n=2.4$) and the refractive index of polyethylene (assuming the value of the
207 pristine material, $n=1.5$) and an incidence angle of 45° . In our case, the calculated
208 effective penetrations are of the order of 2.5μ for the frequencies of interest, but we
209 calculated them explicitly as a function of the frequency, thus taking into account the
210 slight difference in penetration depth of the beam at different frequencies. We note that
211 the effective penetration depth is then markedly smaller than the critical thickness for

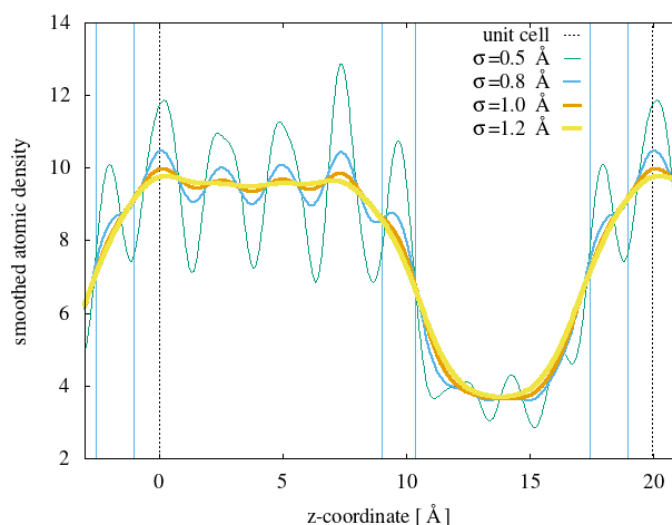


Figure 2. Planar average atomic density along the z direction (perpendicular to lamella surfaces) for the model shown in Fig. 1. The various curves have been obtained with different choices of the width σ for the gaussian function representing each atom. The region considered as "surface" in the following is delimited by blue vertical lines. Dotted lines are the boundaries of the periodic cell.

212 oxygen diffusion mentioned above, assuring thus the homogeneity of the oxidation in
 213 the analysed region.

214 For the ϵ values, those that were not available from experiments, were supplied by
 215 theoretical values extracted from our calculated IR activities (see section 2.2), assuming,
 216 for a given species i , $\epsilon_i = \epsilon_{ketone}^{exp} \times \frac{\epsilon_i^{theo}}{\epsilon_{ketone}^{theo}}$. The used values will be presented in section
 217 3.2.

218 3. Results and discussion

219 3.1. Analysis of experimental FTIR spectra

220 Figure 3 presents the deconvolution results obtained for LLDPE irradiated at 50
 221 and 100 kGy; the numerical details are given in Table 3. Analogous results for XLPE
 222 irradiated at 50 kGy and 100 kGy are presented in Figure 4 and Table 4.

223 The main goal of the deconvolutions is to estimate the relative concentrations of
 224 the various chemical species produced under irradiation, which can help understanding
 225 the kinetic mechanisms driving the degradation of polyethylene under irradiation. To
 226 extract concentrations from the parameters of the gaussian functions outcome of the
 227 fitting procedure, one has to consider that the molar extinction coefficient ϵ of the various
 228 species are potentially different. Moreover, as we will see, some questions remain about
 229 the identification/assignment of the frequencies and IR intensity associated with the
 230 various experimental peaks. For this reason we first present the theoretical results that
 231 we obtained, which can, in some cases, provide missing (or alternative) data for the
 232 analysis of the experimental results.

233 3.2. Calculated IR spectra

234 To support the interpretation of the measured FTIR spectra we calculated, using
 235 DFPT, the infrared spectra of several carbonyl species, inserted in our lamellar model
 236 at various possible insertion sites. These include crystalline bulk sites, carbonyls at
 237 carbon atoms sitting on the lamellar surface, or on the chain in the low density region
 238 mimicking the amorphous fraction of the polymer. We focus here on the carbonyl region
 239 of the spectrum. The absolute value of the calculated frequencies is generally a few tens
 240 of cm^{-1} lower than expected frequencies. This probably comes from the approximations

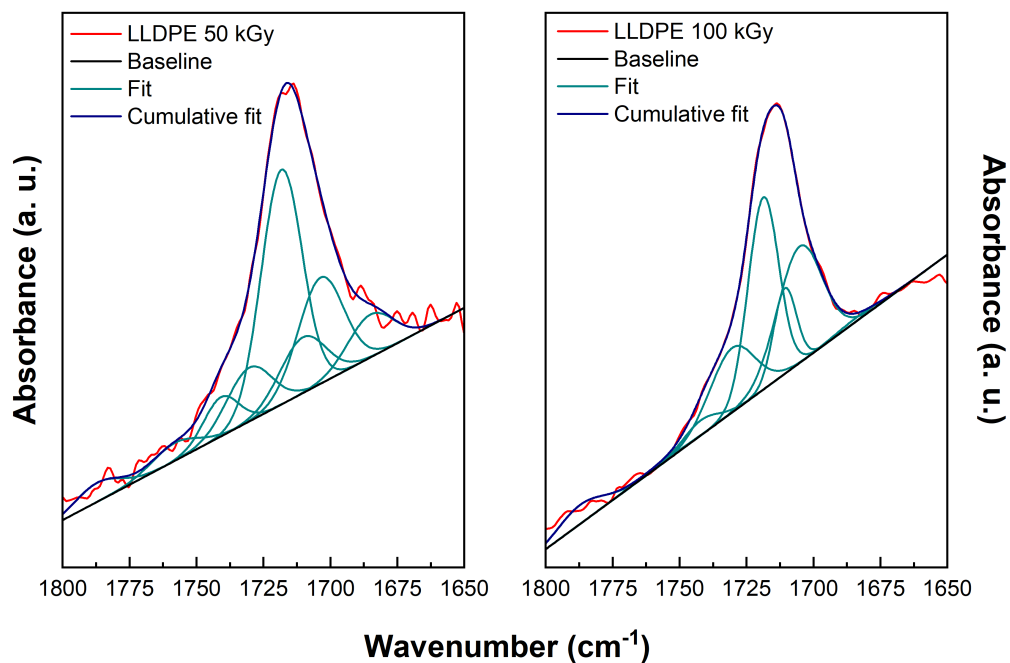


Figure 3. Deconvolution results for LLDPE irradiated at 50 kGy (left) and 100 kGy (right). FWHM of the fitting gaussians are constrained between 10 and 20 cm^{-1} . The corresponding numerical results given in Table 3.

Table 3: Numerical results of the deconvolution for LLDPE irradiated at 50 kGy (left) and 100 kGy (right). Constraints on peak positions ν are in Table 2. FWHM of the fitting gaussians are constrained between 10 and 20 cm^{-1} .

FTIR band attribution	ν_{exp}^* [cm^{-1}]	LLDPE 50 kGy			LLDPE 100 kGy		
		ν	height	FWHM	ν	height	FWHM
Lactone	1785	1787	1.20×10^{-4}	20	1787	3.1^{-4}	20
Ketone+alcohol	1706	1704	6.70×10^{-4}	20	1705	0.00189	19.5
Carboxyle	1756	1758	1.12×10^{-4}	20	1758	$\simeq 2.95 \times 10^{-5}$	20
Ester	1740	1741	2.47×10^{-4}	15.4	1742	2.45×10^{-4}	15.4
Aldehyde	1730	1730	3.39×10^{-4}	19.7	1730	0.00104	19.6
Ketone	1718	1718	0.00148	18	1719	0.00312	13.5
H-bonded	1710	1710	3.52×10^{-4}	20	1711	0.00139	10
Carboxile	1685	1685	2.70×10^{-4}	20	1683	6.08×10^{-5}	19.6
Conj. ketone							

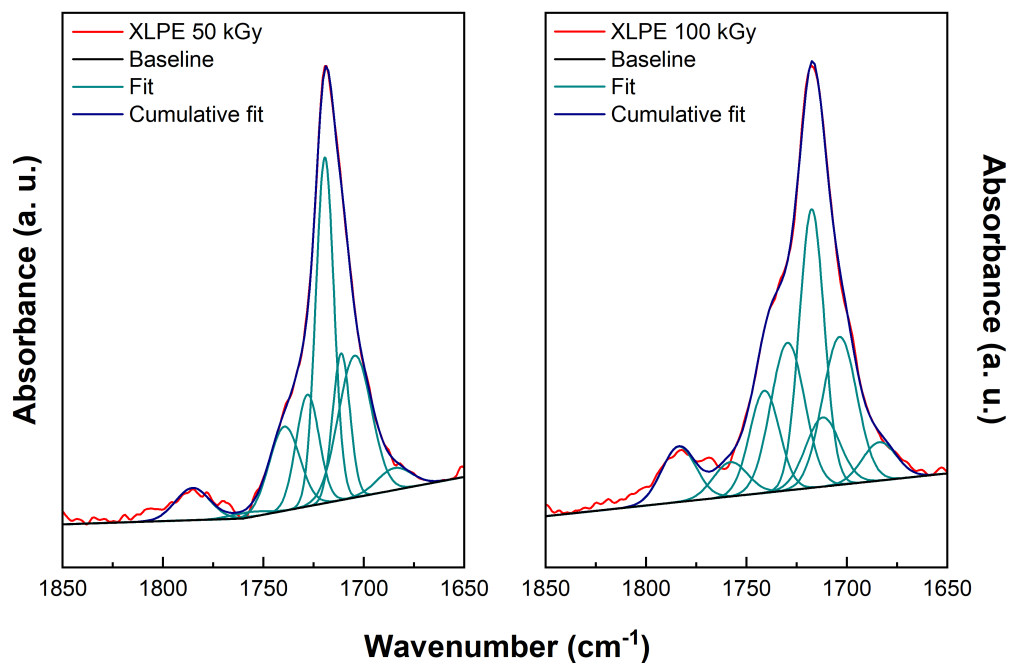


Figure 4. Deconvolution results for XLPE irradiated at 50 kGy (left) and 100 kGy (right). FWHM of the fitting gaussians are constrained between 10 and 20 cm^{-1} . Associated numerical results given in Table 4.

Table 4: Numerical results of the deconvolution for XLPE irradiated at 50 kGy (left) and 100 kGy (right). Constraints on peak positions ν are in Table 2. FWHM of the fitting gaussians are constrained between 10 and 20 cm^{-1} .

FTIR band attribution	ν_{exp}^* [cm^{-1}]	XLPE 50 kGy			XLPE 100 kGy		
		ν	height	FWHM	ν	height	FWHM
Lactone	1785	1785	7.27×10^{-4}	20	1784	0.00175	20
Ketone+alcohol	1706	1705	0.0032	19.4	1704	0.00467	20
Carboxyle	1756	1758	1.21×10^{-4}	20	1758	0.00108	20
Ester	1740	1740	0.0019	17.8	1741	0.00322	17.3
Aldehyde	1730	1728	0.00252	13.5	1730	0.00466	19.7
Ketone	1718	1719	0.00779	10.6	1718	0.00879	14.5
H-bonded carboxyle	1710	1711	0.0033	10.1	1712	0.00218	20
Conjugated ketone	1685	1685	4.95×10^{-4}	20	1684	0.00121	20

Table 5: Comparison of theoretical (average) frequencies and IR activities with the corresponding experimental values (frequencies and ϵ are extracted, for each species, from the references mentioned in table 2). The calculated quantities are averaged over a number of insertion sites of the carbonyl in the lamellar model. The standard deviation of the frequencies and of the IR activities are given in parenthesis.

	ν_{th}^* [cm^{-1}]	ν_{exp}^* [cm^{-1}]	IR activity [$(\text{D}/\text{\AA})^2\text{amu}^{-1}$]	ϵ [$\text{L mol}^{-1}\text{cm}^{-1}$]
Lactone	–	1785	–	720[41]
Ester	1684 (9.4)	1740	10.99 (1.422)	450[42]
Ketone	1672 (9.9)	1718	7.02 (0.827)	300[42]
Aldehyde	1702 (5.1)	1734	7.25 (1.313)	235[23]
Carboxylic Acid (free)	1711 (3.7)	1756	11.50 (2.571)	516[23]
H-bonded Carboxylic acid	–	1710	–	680[42]
Conjugated Ketone	1658 (16.3)	1685	5.10 (1.659)	388[23]
Ketone+Alcohol	1664 (12.1)	–	6.99 (1.291)	–

241 used, but might also partly depend on the role of the local atomic environment. As a
 242 support to the comparison of experimental and theoretical frequencies, we provide in
 243 the Supplementary Information further results of calculations for isolated molecules,
 244 compared to experimental results obtained for gas, liquid phases or solutions.

245 However, more than on the absolute value, we focus here on the spread of the
 246 frequency for a single species as a function of the position of the carbonyl in the lamellar
 247 model. The absolute value of the calculated frequencies are generally on the order of
 248 30 cm^{-1} lower than the experimental values presented in Table 2. We summarise in
 249 table 5 the average values of calculated frequencies and IR activities and their standard
 250 deviation. From the latter one can extract the corresponding FWHM of a corresponding
 251 gaussian distribution, that can be compared with the constraints given in the deconvol-
 252 ution procedure. As an example, the calculated FWHM is $\sim 22 \text{ cm}^{-1}$ for ketones, \sim
 253 23 cm^{-1} for esters, $\sim 9 \text{ cm}^{-1}$ for carboxylic acids, and 38 cm^{-1} for conjugated ketones,
 254 although for the latter two species we have only few data.

255 The discrepancies between theoretical and experimental frequencies is on the order
 256 of generally proposed correction factors for quantum chemical calculations of vibrational
 257 frequencies [25] for molecules; a scale factor of 1.025 applied to theoretical frequencies
 258 would bring them in fair agreement with the experimental reference values. We note
 259 that we compared our theoretical carboxylic acid to the free carboxylic acid of table 2,
 260 and not to the H-bonded variant, whose experimentally determined frequency would
 261 perfectly match our theoretical value. In this respect we performed some tests for small
 262 molecules and our theoretical prediction of the vibrational frequency of propionic acid
 263 (1772 cm^{-1}) is in fairly good agreement with NIST gas-phase results [43], without the
 264 application of the scale factor. This suggests that the role of the local atomic environment
 265 and the intermolecular interactions on the characteristic frequencies are still to be fully
 266 understood.

267 We now analyse the theoretical results, both the frequencies and intensities, accord-
 268 ing to the position of the carbonyl species in the unit cell. To this goal we now present in
 269 a graphical form (figure 5) the results already summarised in table 5, through average
 270 values and standard deviations.

271 The results, within the limit of our model, do not show a strong difference in
 272 dispersions, both of frequencies and IR activities, versus the position. However, in
 273 particular for esters, the dispersion in the bulk seems a bit less pronounced than on
 274 the surface and the low density (amorphous like) region. Figure 6 shows also that the
 275 dispersion of the intensities seems much larger for esters and carboxylic acids than for

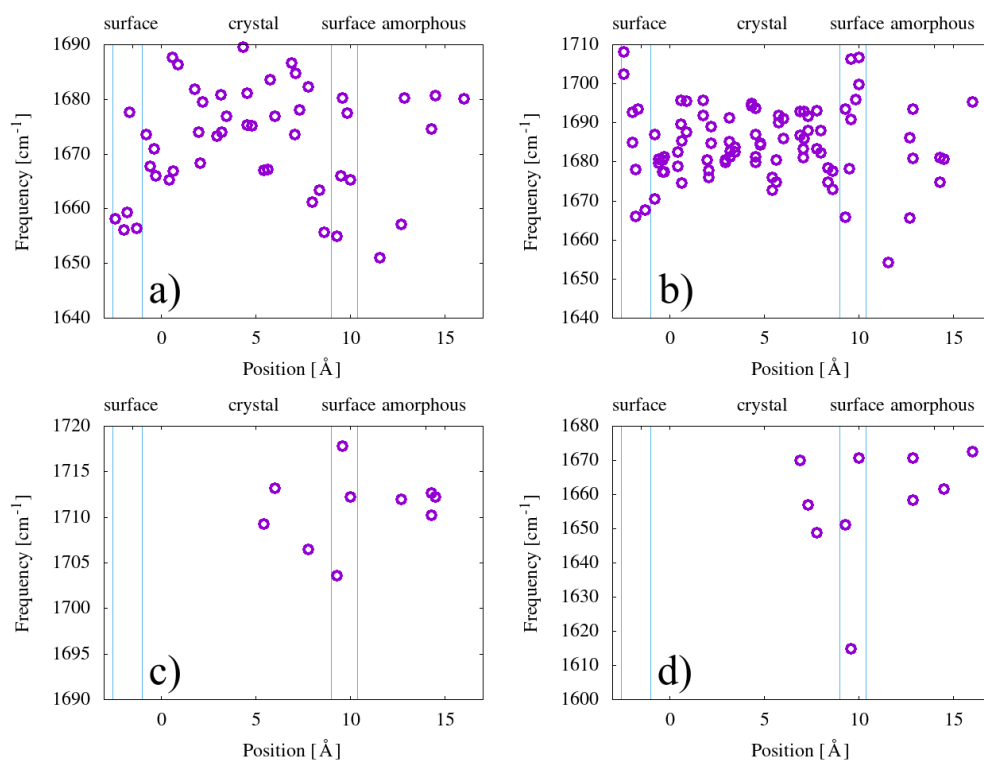


Figure 5. Calculated frequencies of the carbonyl group for a) ketones, b) esters, c) carboxylic acids, d) enones, presented as a function of the position in the simulation cell in the direction perpendicular to the lamellæ. Vertical blue lines delimit regions identified as amorphous, crystalline, and surface, as shown on top of the graph.

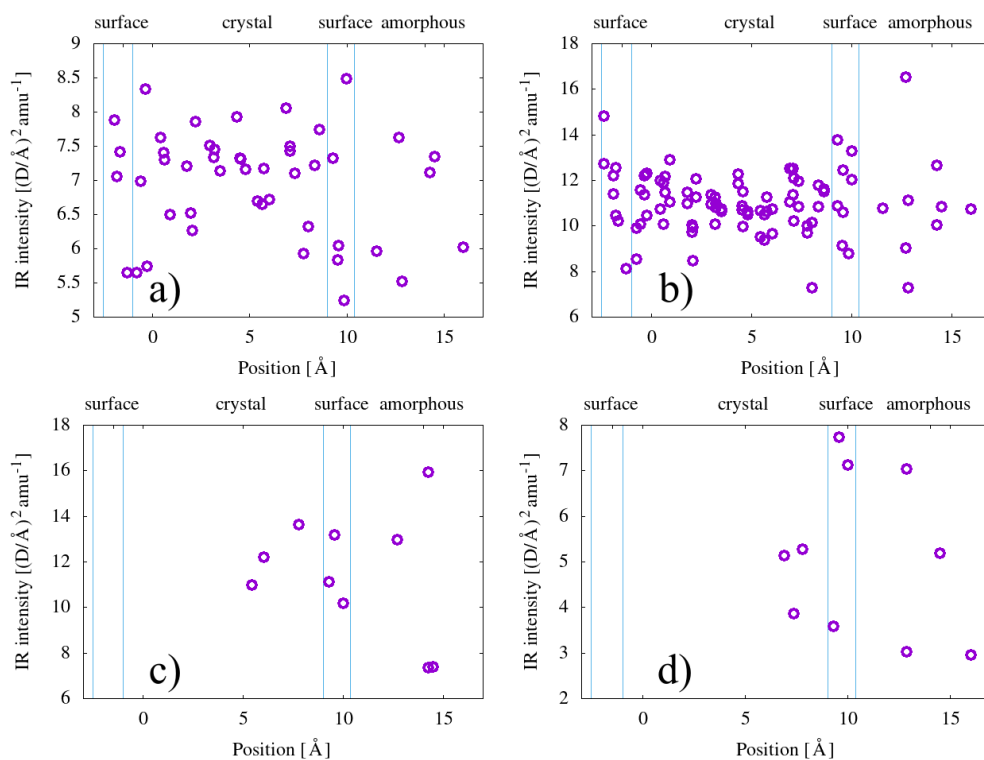


Figure 6. Calculated infrared activities of the carbonyl group for a) ketones, b) esters, c) carboxylic acids, d) enones, presented as a function of the position in the simulation cell in the direction perpendicular to the lamellæ. Vertical blue lines delimit regions identified as amorphous, crystalline, and surface, as shown on top of the graph.

ketones and enones. We note that we do not find any clear sign of correlation between the frequency and the IR activity of the calculated configurations.

We choose to present the theoretical results for frequencies and IR activities obtained with our lamellar model as a function of the position of the carbonyl in the model structure, in particular as a function of the distance with respect to the lamella surface. The idea is to understand if it could be possible, in principle, to distinguish through the IR signal the position of the carbonyls, even if we know that it is generally admitted that oxygen molecules cannot penetrate and thus induce carbonyl formation inside the crystalline regions. If, however, for some reason some oxygen happens to be trapped in a crystalline environment, or able to penetrate it, our results do not support the idea that inside the crystal the frequency values are less dispersed than in the amorphous region, and thus distinguishable in any way. It is true that the lamella in our model is much thinner than real crystalline lamellae in polyethylene, but we stress also the importance of being able to simulate phenomena at the interface between amorphous and crystal phases, which constitute a relevant fraction of the material [44,45]; moreover, at lamellae surfaces, at least some of the relevant reactions involved in PE ageing and carbonyl production may take place easier than elsewhere [37].

Let us come now to the dispersion of frequencies as calculated for every single carbonyl type. We note that the gaussian width allowed in experimental deconvolution procedures ($10\text{-}20\text{ cm}^{-1}$) are coherent with what we find from our multiple calculations; at least for ketones and esters, for which we have a sufficiently large set of calculated data. This confirms that the origin of the width of infrared peaks associated to each carbonyl type has to be attributed to the variety of local atomic environments available, although not necessarily due to the amorphous nature of the region where carbonyls are formed: for surface and subsurface regions we predict similar dispersions.

If we analyse the comparison of theoretical and experimental frequencies of IR active modes, first we note that the theoretical spectrum of our PE model is globally in good agreement with experiments (see Supplementary information), although with a slight overestimation (1.7%) of the C-H stretching doublet at $2850\text{-}2925\text{ cm}^{-1}$ and a similar underestimation (1.2%) of the bending modes around $1450\text{-}1500\text{ cm}^{-1}$. Concerning the IR active C=O stretching mode used to probe carbonyl species, the underestimation seems to be a bit larger according to table 5, yet quite satisfactory for DFT calculations of this kind. We performed similar calculations for small molecules containing similar C=O bonds and we obtained results which are, in some cases, in even better agreement with the experiment (see Supplementary Information). However, we stress that the choice of the experimental reference value is not always straightforward, even for such small molecules, whose frequency can change significantly according to the investigated phase (gas, liquid, solution). Variations might possibly be expected also between PE samples with different density, additives, and carbonyl concentrations. In order to estimate concentrations, however, we need an even better match with experimental frequencies, thus we chose to scale the theoretical frequencies with a factor (1.025) which brings them close to experimental results (almost minimizing the standard deviation of the error distribution), keeping however the theoretical ratio between frequencies of different carbonyls.

A last note on the inclusion, between the various carbonyl species, of ketone+alcohol pairs, for which we do not have an experimental reference. In a recent paper assessing the viability of various reaction paths through energy barrier calculations [37], we suggest that a relevant ketone production mechanism leads to such pairs. Our calculations of vibrational modes shows a slight decrease in the average frequency and, thus, we think it is interesting to include them in the deconvolution procedure.

3.3. Concentrations of carbonyl species

The obtained concentrations are shown in figure 7. Here we compare three sets of concentrations, of which the first was obtained uniquely from experimental estimations

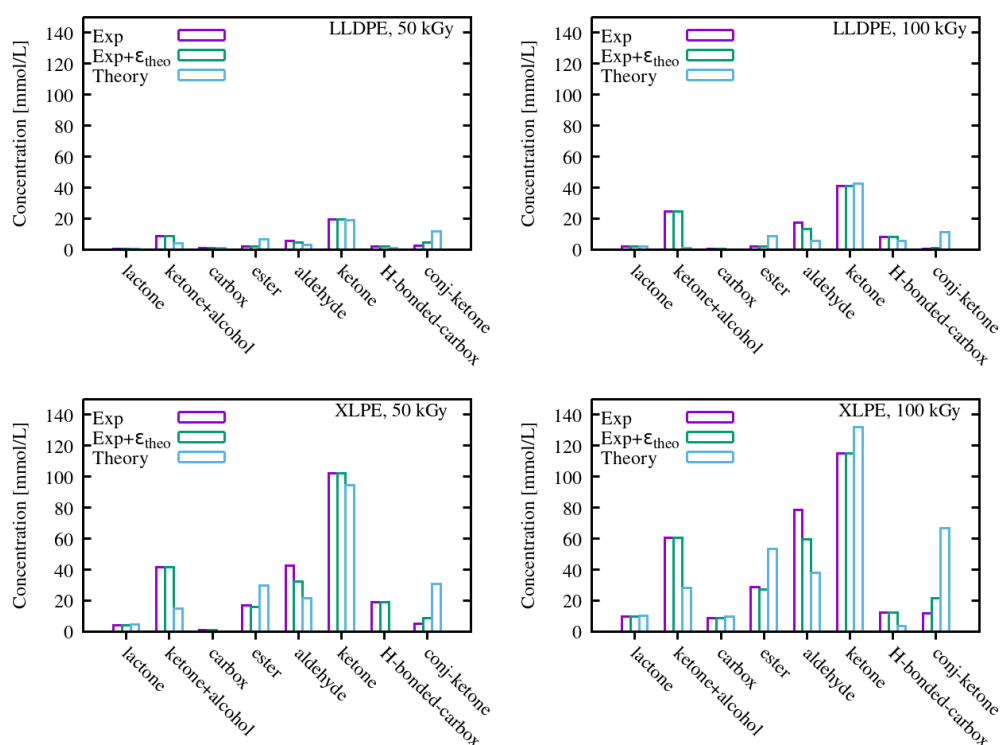


Figure 7. Concentrations of various species as determined from FTIR spectra deconvolution for LLDPE and XLPE for two irradiation doses. We show concentrations obtained with three different sets of fitting parameters, coming only from experiments (“Exp”), only from theory (“Theory”), or from a combination of them (“Exp+ ϵ_{theo} ”).

329 of peak heights and extinction coefficients, the second is issued from a combination of
 330 experimental peak heights and theoretical IR activities/ ϵ , and the third was obtained
 331 using peak heights from a deconvolution based on theoretical frequencies, combined
 332 with theoretical IR activities (except for lactones and H-bonded carboxylic acids, which
 333 were not in our calculated set). We note that the main outcomes are qualitatively
 334 similar for the three sets of concentrations: ketones are the dominant carbonyl type
 335 for both material types and doses, as expected from several previous results on similar
 336 materials [22,46–48]. Second, the build up of carbonyl species is significantly larger for
 337 XLPE than for LLDPE. Third, other species whose concentration is non-negligible are
 338 esters, aldehydes, lactones, and conjugated ketones.

339 For the latter, we note the first clear peculiarity of the concentrations obtained
 340 uniquely from theoretical frequencies and IR activities: a much higher concentration
 341 of enones (α , β -conjugated ketones), which is probably due to two factors: the relative
 342 frequency with respect to other species (closer to ketones in the theoretical frequency
 343 set) and the lower relative value of the absorption coefficient in the theoretical set with
 344 respect to the experimental one. For the latter, the reference experimental value was
 345 obtained for propiophenone, an aromatic compound which is, in fact, different from our
 346 enone.

347 The other main difference is the prevalence of esters over aldehydes in the theo-
 348 retical analysis, in contrast with the experimental one. This comes not only from the
 349 different extinction coefficients, but also from the inversion of the frequency ordering
 350 between the two species. The fact that, theoretically, we find a slightly higher frequency
 351 for aldehydes than for esters is not excluded by the experimental results presented
 352 in Ref. [23]. This is not without consequences in assessing the ageing mechanisms in
 353 polyethylene, because the presence of aldehydes is directly related to the occurring of
 354 β -scission reactions [49], possibly triggered by alkoxy radicals [37]. Esters, on their side,

355 require beforehand the presence of ketone groups which are attacked by alkoxy radicals
356 [50]. As products of secondary reactions, their concentration could be expected to be
357 lower than the one of aldehyde groups.

358 The concentration of ketone+alcohol pairs, which, even in the experimental set of
359 reference data is the only one which is, in fact, coming from our calculations, seems to be
360 in competition with conjugated ketones in the lower frequency section of the carbonyl
361 signal. A larger separation (in frequency) between ketones and ketone+alcohol pairs
362 clearly enhances the calculated concentration of the latter, at the expense of conjugated
363 ketones, which represent the lowest frequency of the fitting set. Nevertheless, even in the
364 fully theoretical set, where ketone and ketone-alcohol pairs are very close in frequency
365 (and then in competition in the deconvolution procedure) their concentration is non
366 negligible, which suggests they cannot be overlooked.

367 The results, in spite of some discrepancies, show that using the outcome of DFT cal-
368 culations can be a valuable tool to complement experimental reference data in analysing
369 experimental spectra of aged polymers, and can contribute to a necessary critical assess-
370 ment [23] of those reference data, especially concerning the absorption coefficients of
371 various species. The theoretical model of PE used in this paper is a rather simplified one,
372 and yet it contains the main ingredients of the complex microstructure of a semicrys-
373 talline polymer. Such feature is important in order to be able to estimate the influence of
374 the local atomic environment on properties, like bond stretching frequencies and dipole
375 moment derivatives, which are fairly local in nature, but not as much so as to guarantee
376 that they can be simulated by isolated molecules in the gas phase.

377 4. Summary and Conclusions

378 In summary, we have analysed the carbonyl degradation products in two polyethy-
379 lene variants (LLDPE and XLPE) using FTIR spectroscopy. Our analysis of experimental
380 infrared spectra, collected on γ -irradiated samples at two doses, combines usual decon-
381 volution procedures and experimental reference data with an extended first principles
382 study of the infrared spectra of various carbonyl species in a model atomic structure.

383 Our model contains structural features of the crystalline, the amorphous phases and
384 the interface between them. The theoretical results, in spite of a slight underestimation
385 of the frequency of the carbonyl signals, well inside the expected accuracy of the method,
386 provide reliable infrared activities that can complement experimental estimation in the
387 exploitation of experimental spectra. The spread in frequencies according to the atomic
388 site where the carbonyl is inserted gives an insight into the influence of the local atomic
389 structure (amorphous, lamella surface, crystal) on the frequencies and IR activities and
390 can be compared to those extracted from deconvolution of experimental spectra.

391 The estimation of the concentration of carbonyls of various types based on, uniquely,
392 theoretical data are compared to the outcome of a fully experimental procedure, showing
393 global agreement. Some differences in the ratio of aldehyde to esters, and the contribu-
394 tion of conjugated ketones, raises the question of the contribution of these species in PE
395 ageing under radio-oxidation. Another carbonyl variant which should be further investi-
396 gated, and which is not systematically included in FTIR analysis of irradiated polyolefins,
397 is a combination of a ketone with an alcohol, as a result of a reaction involving alkoxy
398 radicals.

399 In conclusion, we think that the approach presented here, combining experimental
400 and theoretical infrared spectra, potentially enhances the capability of FTIR spectroscopy
401 to distinguish and quantify degradation products present in polymers undergoing
402 ageing processes. This method can be easily applied to other polymers, provided a
403 representative atomic model is conceived.

404 **Author Contributions:** Conceptualization, M.F., G.R., and Y.N.; methodology, M.F. and G.R.; soft-
405 ware, G.R. and Y.A.; validation, M.F., G.R., and Y.N.; formal analysis, M.F. and G.R.; investigation,
406 M.F., G.R., F.L.D., Y.A.; resources, M.F., G.R.; data curation, M.F. and G.R.; writing—original draft
407 preparation, M.F. and G.R.; writing—review and editing, G.R., M.F., Y.N., and Y.A.; visualization,

408 G.R. and M.F.; supervision, M.F. and G.R.; project administration, M.F.; funding acquisition, M.F.
409 and G.R. All authors have read and agreed to the published version of the manuscript.

410 **Funding:** This publication was prepared in the context of the Team Cables project. This project
411 has received funding from the Euratom research and training programme 2014–2018 under grant
412 agreement No 755183. This work was granted access to the HPC resources of TGCC and IDRIS
413 under the allocation 2022A0090906018 made by GENCI and under the allocation by CEA-DEN.

414 **Institutional Review Board Statement:** Not applicable

415 **Informed Consent Statement:** Not applicable

416 **Data Availability Statement:** The data presented in this study are available on request from the
417 corresponding author.

418 **Acknowledgments:** This work was granted access to the HPC resources of TGCC and IDRIS
419 under the allocations 2022-A0130906018 and 2021-A0110906018 made by GENCI.



420 The project leading to the work presented here has received funding from the
421 Euratom research and training programme 2014–2018 under grant agreement No.755183.

422 The views expressed here are the responsibility of the author(s) only. The EU Commission
423 takes no responsibility for any use made of the information set out.

424 **Conflicts of Interest:** The authors declare no conflict of interest.

References

1. Geyer, R.; Jambeck, J.R.; Law, K.L. Production, use, and fate of all plastics ever made. *Sci. Adv.* **2017**, *3*, e1700782.
2. Ghatge, S.; Yang, Y.; Ahn, J.H.; Hur, H.G. Biodegradation of polyethylene: a brief review. *Applied Biological Chemistry* **2020**, *63*, 27. doi:10.1186/s13765-020-00511-3.
3. Ferry, M.; Roma, G.; Cochon, F.; Esnouf, S.; Dauvois, V.; Nizeyimana, F.; Gervais, B.; Ngono-Ravache, Y. 3.16 - Polymers in the Nuclear Power Industry. In *Comprehensive Nuclear Materials (Second Edition)*, Second Edition ed.; Konings, R.J.; Stoller, R.E., Eds.; Elsevier: Oxford, 2020; pp. 545–580. doi:https://doi.org/10.1016/B978-0-12-803581-8.11616-9.
4. Ferry, M.; Pellizzi, E.; Boughattas, I.; Fromentin, E.; Dauvois, V.; de Combarieu, G.; Coignet, P.; Cochon, F.; Ngono-Ravache, Y.; Balanzat, E.; Esnouf, S. Effect of cumulated dose on hydrogen emission from polyethylene irradiated under oxidative atmosphere using gamma rays and ion beams. *Radiation Physics and Chemistry* **2016**, *118*, 124–127. Ionizing Radiation and Polymers symposium, IRaP 2014, doi:https://doi.org/10.1016/j.radphyschem.2015.06.006.
5. Seguchi, T.; Arakawa, K.; Hayakawa, N.; Machi, S. Radiation induced oxidative degradation of polymers—IV. Dose rate effects on chemical and mechanical properties. *Radiation Physics and Chemistry (1977)* **1981**, *18*, 671–678. doi:https://doi.org/10.1016/0146-5724(81)90190-4.
6. Reynolds, A.; Bell, R.; Bryson, N.; Doyle, T.; Hall, M.; Mason, L.; Quintric, L.; Terwilliger, P. Dose-rate effects on the radiation-induced oxidation of electric cable used in nuclear power plants. *Radiation Physics and Chemistry* **1995**, *45*, 103–110. doi:https://doi.org/10.1016/0969-806X(94)E0003-2.
7. Sidi, A.; Colombani, J.; Larché, J.F.; Rivaton, A. Multiscale analysis of the radiooxidative degradation of EVA/EPDM composites. ATH filler and dose rate effect. *Radiation Physics and Chemistry* **2018**, *142*, 14–22. Ionizing Radiations and Polymers, IRaP-2016, doi:https://doi.org/10.1016/j.radphyschem.2017.04.007.
8. Suraci, S.V.; Amat, S.; Hippolyte, L.; Malechaux, A.; Fabiani, D.; Le Gall, C.; Juan, O.; Dupuy, N. Ageing evaluation of cable insulations subjected to radiation ageing: Application of principal component analyses to Fourier Transform Infra-Red and dielectric spectroscopy. *High Voltage* **2022**, *7*, 652–665, [https://ietresearch.onlinelibrary.wiley.com/doi/pdf/10.1049/hve2.12239]. doi:https://doi.org/10.1049/hve2.12239.
9. Fessenden, R.W.; Schuler, R.H. Electron Spin Resonance Studies of Transient Alkyl Radicals. *The Journal of Chemical Physics* **1963**, *39*, 2147–2195, [https://doi.org/10.1063/1.1701415]. doi:10.1063/1.1701415.
10. Keyser, R.M.; Tsuji, K.; Williams, F. Trapped Electrons in γ -Irradiated Polyethylene Identified by Electron Spin Resonance Spectroscopy. *Macromolecules* **1968**, *1*, 289–290, [https://doi.org/10.1021/ma60003a018]. doi:10.1021/ma60003a018.
11. Hikmet, R.; Keller, A. Crystallinity dependent free radical formation and decay in irradiated polyethylene in the presence of oxygen. *International Journal of Radiation Applications and Instrumentation. Part C. Radiation Physics and Chemistry* **1987**, *29*, 15–19. doi:https://doi.org/10.1016/1359-0197(87)90055-5.
12. Salih, M.; Buttafava, A.; Ravasio, U.; Mariani, M.; Fautitano, A. EPR investigation on radiation-induced graft copolymerization of styrene onto polyethylene: Energy transfer effects. *Radiation Physics and Chemistry* **2007**, *76*, 1360–1366. Proceedings of the 11th Tihany Symposium on Radiation Chemistry, doi:https://doi.org/10.1016/j.radphyschem.2007.02.032.
13. Przybytniak, G.; Sadło, J.; Walo, M.; Wróbel, N.; Žák, P. Comparison of radical processes in non-aged and radiation-aged polyethylene unprotected or protected by antioxidants. *Materials Today Communications* **2020**, *25*, 101521. doi:https://doi.org/10.1016/j.mtcomm.2020

14. Osawa, Z.; Kuroda, H. Differences in polyene formation between polyethylene and polypropylene during photo-irradiation. *Polymer Photochemistry* **1986**, *7*, 231–236. doi:[https://doi.org/10.1016/0144-2880\(86\)90029-1](https://doi.org/10.1016/0144-2880(86)90029-1).
15. Teyssedre, G.; Cissé, L.; Laurent, C.; Massines, F.; Tiemblo, P. Spectral Analysis of Optical Emission Due to Isothermal Charge Recombination in Polyolefins. *IEEE Transactions on Dielectrics and Electrical Insulation* **1998**.
16. Randall, J.; Zoepfl, F.; Silverman, J. High-resolution solution carbon 13 NMR measurements of irradiated polyethylene. *Radiation Physics and Chemistry (1977)* **1983**, *22*, 183–192. doi:[https://doi.org/10.1016/0146-5724\(83\)90202-9](https://doi.org/10.1016/0146-5724(83)90202-9).
17. Palmas, P.; Le Campion, L.; Bourgeoisat, C.; Martel, L. Curing and thermal ageing of elastomers as studied by 1H broadband and 13C high-resolution solid-state NMR. *Polymer* **2001**, *42*, 7675–7683. doi:[https://doi.org/10.1016/S0032-3861\(01\)00249-X](https://doi.org/10.1016/S0032-3861(01)00249-X).
18. Fallgatter, M.B.; Dole, M. The Radiation Chemistry of Polyethylene. VII. Polyene Formation1. *The Journal of Physical Chemistry* **1964**, *68*, 1988–1997, [<https://doi.org/10.1021/j100789a053>]. doi:10.1021/j100789a053.
19. Mailhot, B.; Gardette, J.L. Polystyrene photooxidation. 2. A pseudo wavelength effect. *Macromolecules* **1992**, *25*, 4127–4133, [<https://doi.org/10.1021/ma00042a013>]. doi:10.1021/ma00042a013.
20. Möller, K.; Gevert, T. A solid-state investigation of the desorption/evaporation of hindered phenols from low density polyethylene using FTIR and UV spectroscopy with integrating sphere: The effect of molecular size on the desorption. *Journal of Applied Polymer Science* **1996**, *61*, 1149–1162.
21. Rivaton, A.; Cambon, S.; Gardette, J.L. Radiochemical ageing of EPDM elastomers.: 2. Identification and quantification of chemical changes in EPDM and EPR films γ -irradiated under oxygen atmosphere. *Nuclear Instruments and Methods in Physics Research Section B: Beam Interactions with Materials and Atoms* **2005**, *227*, 343–356. doi:<https://doi.org/10.1016/j.nimb.2004.09.008>.
22. Gardette, M.; Perthue, A.; Gardette, J.L.; Janecska, T.; Földes, E.; Pukánszky, B.; Therias, S. Photo- and thermal-oxidation of polyethylene: Comparison of mechanisms and influence of unsaturation content. *Polymer Degradation and Stability* **2013**, *98*, 2383–2390. doi:<https://doi.org/10.1016/j.polymdegradstab.2013.07.017>.
23. Celina, M.C.; Linde, E.; Martinez, E. Carbonyl Identification and Quantification Uncertainties for Oxidative Polymer Degradation. *Polymer Degradation and Stability* **2021**, *188*, 109550. doi:<https://doi.org/10.1016/j.polymdegradstab.2021.109550>.
24. Baroni, S.; de Gironcoli, S.; Dal Corso, A.; Giannozzi, P. Phonons and related crystal properties from density-functional perturbation theory. *Rev. Mod. Phys.* **2001**, *73*, 515.
25. Schott, A.P.; Radom, L. Harmonic Vibrational Frequencies: An Evaluation of Hartree-Fock, Moller-Plesset, Quadratic Configuration Interaction, Density Functional Theory, and Semiempirical ScaleFactors. *J. Phys. Chem.* **1996**, *100*, 16502.
26. Porezag, D.; Pederson, M.R. Infrared intensities and Raman-scattering activities within density-functional theory. *Phys. Rev. B* **1996**, *54*, 7830. Publisher: American Physical Society, doi:10.1103/PhysRevB.54.7830.
27. Halls, M.D.; Schlegel, H.B. Comparison of the performance of local, gradient-corrected, and hybrid density functional models in predicting infrared intensities. *The Journal of Chemical Physics* **1998**, *109*, 10587–10593, [<https://doi.org/10.1063/1.476518>]. doi:10.1063/1.476518.
28. Gaigeot, M.P.; Sprik, M. Ab Initio Molecular Dynamics Computation of the Infrared Spectrum of Aqueous Uracil. *J. Phys. Chem. B* **2003**, *107*, 10344.
29. Welch, M.D.; Montgomery, W.; Balan, E.; Lerch, P. Insights into the high-pressure behavior of kaolinite from infrared spectroscopy and quantum-mechanical calculations. *Physics and Chemistry of Minerals* **2012**, *39*, 143–151. doi:10.1007/s00269-011-0469-5.
30. Ferry, M.; Carpentier, F.; Cornaton, M. Radio-Oxidation Ageing of XLPE Containing Different Additives and Filler: Effect on the Gases Emission and Consumption. *Polymers* **2021**, *13*. doi:10.3390/polym13172845.
31. Gillen, K.T.; Clough, R.L., Quantitative Confirmation of Simple Theoretical Models for Diffusion-Limited Oxidation. In *Radiation Effects on Polymers*; American Chemical Society, 1991; chapter 28, pp. 457–472, [<https://pubs.acs.org/doi/pdf/10.1021/bk-1991-0475.ch028>]. doi:10.1021/bk-1991-0475.ch028.
32. Ngonon-Ravache, Y.; Damaj, Z.; Dannoux-Papin, A.; Ferry, M.; Esnouf, S.; Cochin, F.; De Combarieu, G.; Balanzat, E. Effect of swift heavy ions on an EPDM elastomer in the presence of oxygen: LET effect on the radiation-induced chemical ageing. *Polymer Degradation and Stability* **2015**, *111*, 89–101. doi:<https://doi.org/10.1016/j.polymdegradstab.2014.10.013>.
33. Boullier, I. Etude du comportement de polyolefines et de polymeres fluores dans des conditions de vieillissement naturel et accelere. PhD thesis, Université des Antilles et de la Guyane, 2000. Thèse de doctorat dirigée par Dupont, Michel Sciences et techniques Antilles-Guyane 2000.
34. Lacoste, J.; Carlsson, D.J. Gamma-, photo-, and thermally-initiated oxidation of linear low density polyethylene: A quantitative comparison of oxidation products. *Journal of Polymer Science Part A: Polymer Chemistry* **1992**, *30*, 493–500, [<https://onlinelibrary.wiley.com/doi/pdf/10.1002/pola.1992.080300316>]. doi:<https://doi.org/10.1002/pola.1992.080300316>.
35. Luongo, J.P. Infrared study of oxygenated groups formed in polyethylene during oxidation. *Journal of Polymer Science* **1960**, *42*, 139–150, [<https://onlinelibrary.wiley.com/doi/pdf/10.1002/pol.1960.1204213916>]. doi:<https://doi.org/10.1002/pol.1960.1204213916>.
36. Teissèdre, G.; Pilichowski, J.; Lacoste, J. Photoageing of polyolefins. I. Photolysis of low molecular weight hydroperoxide at $\lambda \geq 300$ nm. *Polymer Degradation and Stability* **1994**, *45*, 145–153. doi:[https://doi.org/10.1016/0141-3910\(94\)90190-2](https://doi.org/10.1016/0141-3910(94)90190-2).
37. Ahn, Y.; Roma, G.; Colin, X. Elucidating the Role of Alkoxy Radicals in Polyethylene Radio-Oxidation Kinetics. *Macromolecules* **2022**, *55*, 8676–8684, [<https://doi.org/10.1021/acs.macromol.2c01135>]. doi:10.1021/acs.macromol.2c01135.
38. Klimeš,.; Bowler, D.R.; Michaelides, A. Van der Waals density functionals applied to solids. *Phys. Rev. B* **2011**, *83*, 195131. Publisher: American Physical Society, doi:10.1103/PhysRevB.83.195131.

39. Roma, G.; Bruneval, F.; Martin-Samos, L. Optical Properties of Saturated and Unsaturated Carbonyl Defects in Polyethylene. *J. Phys. Chem. B* **2018**, *122*, 2023–2030, [<https://doi.org/10.1021/acs.jpcc.7b12172>]. doi:<https://dx.doi.org/10.1021/acs.jpcc.7b12172>.
40. Giannozzi, P.; Baroni, S.; Bonini, N.; Calandra, M.; Car, R.; Cavazzoni, C.; Ceresoli, D.; Chiarotti, G.L.; Cococcioni, M.; Dabo, I.; Corso, A.D.; Gironcoli, S.d.; Fabris, S.; Fratesi, G.; Gebauer, R.; Gerstmann, U.; Gougoussis, C.; Kokalj, A.; Lazzeri, M.; Martin-Samos, L.; Marzari, N.; Mauri, F.; Mazzarello, R.; Paolini, S.; Pasquarello, A.; Paulatto, L.; Sbraccia, C.; Scandolo, S.; Sclauzero, G.; Seitsonen, A.P.; Smogunov, A.; Umari, P.; Wentzcovitch, R.M. QUANTUM ESPRESSO: a modular and open-source software project for quantum simulations of materials. *J. Phys.: Condens. Matter* **2009**, *21*, 395502.
41. Lacoste, J.; Carlsson, D.; Falicki, S.; Wiles, D. Polyethylene hydroperoxide decomposition products. *Polymer Degradation and Stability* **1991**, *34*, 309–323. Polymer Stabilisation Mechanisms and Applications, doi:[https://doi.org/10.1016/0141-3910\(91\)90125-B](https://doi.org/10.1016/0141-3910(91)90125-B).
42. Carlsson, D.J.; Wiles, D.M. The Photodegradation of Polypropylene Films. II. Photolysis of Ketonic Oxidation Products. *Macromolecules* **1969**, *2*, 587–597, [<https://doi.org/10.1021/ma60012a006>]. doi:10.1021/ma60012a006.
43. Sadtler Research Labs Under US-EPA Contract. NIST Standard Reference Database 35, NIST/EPA Gas-Phase Infrared Database JCAMP Format. Technical report, NIST Mass Spectrometry Data Center, William E. Wallace, director, 2018. doi:10.18434/T4D303.
44. Zhou, H.; Wilkes, G. Comparison of lamellar thickness and its distribution determined from d.s.c., SAXS, TEM and AFM for high-density polyethylene films having a stacked lamellar morphology. *Polymer* **1997**, *38*, 5735–5747. doi:[https://doi.org/10.1016/S0032-3861\(97\)00145-6](https://doi.org/10.1016/S0032-3861(97)00145-6).
45. Savage, R.C.; Mullin, N.; Hobbs, J.K. Molecular Conformation at the Crystal–Amorphous Interface in Polyethylene. *Macromol.* **2015**, *48*, 6160–6165, [<https://doi.org/10.1021/ma5025736>]. doi:10.1021/ma5025736.
46. Fodor, Z.; Iring, M.; Tüdös, F.; Kelen, T. Determination of carbonyl-containing functional groups in oxidized polyethylene. *Journal of Polymer Science: Polymer Chemistry Edition* **1984**, *22*, 2539–2550.
47. Costa, L.; Luda, M.; Trossarelli, L. Ultra high molecular weight polyethylene—II. Thermal and photo-oxidation. *Polymer Degradation and Stability* **1997**, *58*, 41–54.
48. Salvalaggio, M.; Bagatin, R.; Fornaroli, M.; Fanutti, S.; Palmery, S.; Battistel, E. Multi-component analysis of low-density polyethylene oxidative degradation. *Polymer degradation and stability* **2006**, *91*, 2775–2785.
49. Khelidj, N.; Colin, X.; Audouin, L.; Verdu, J.; Monchy-Leroy, C.; Prunier, V. Oxidation of polyethylene under irradiation at low temperature and low dose rate. Part I. The case of “pure” radiochemical initiation. *Polymer Degradation and Stability* **2006**, *91*, 1593–1597. doi:<https://doi.org/10.1016/j.polymdegradstab.2005.09.011>.
50. Cambon, S. Étude du mécanisme de dégradation radiochimique d’un élastomère de type EPDM. PhD thesis, Université de Clermont Ferrand, 2001.